SIAM J. APPLIED DYNAMICAL SYSTEMS
Vol. 9, No. 1, pp. 261–281

Within-Burst Synchrony Changes for Coupled Elliptic Bursters*

Abul Kalam al Azad† and Peter Ashwin†

Abstract. We study a novel phenomenon for coupled identical bursters: synchronized bursts where there are changes of spike synchrony within each burst. The examples we study are for normal form elliptic bursters where there is a periodic slow passage around a Bautin (codimension two degenerate Andronov–Hopf) bifurcation. This burster has a subcritical Andronov–Hopf bifurcation at the onset of repetitive spiking, while the end of burst occurs via a fold limit cycle bifurcation. We study synchronization behavior of two and three Bautin-type elliptic bursters for a linear direct coupling scheme as well as demonstrating the phenomenon in an approximation of gap-junction and synaptic coupling. Burst synchronization is known to be prevalent among such coupled bursters, while spike synchronization is more dependent on the details of the coupling. We note that higher order terms in the normal form that do not affect the behavior of a single burster can be responsible for changes in the synchrony pattern; more precisely, we find within-burst synchrony changes associated with a turning point in the spiking frequency.

Key words. elliptic burster, Bautin bifurcation, normal form, spike synchronization, slow passage effect, gap-junction, synaptic coupling

AMS subject classifications. 37G05, 37G15, 92B25

DOI. 10.1137/090746045

1. Introduction.

Elliptic bursting in a neuronal system is a type of recurrent alternation between active phases (large amplitude oscillations) and quiescent phases (small amplitude oscillations). This kind of rhythmic pattern can be found in rodent trigeminal neurons [16], thalamic relay and reticularis neurons [5, 6], the primary afferent neurons in brain stem circuits [19], and neurons in many other areas of the brain. It is clearly of interest for neuronal population information encoding and transmission where several bursters fire within a population. Patterns of synchrony of elliptic bursters may also be helpful in understanding firing patterns in more general types of burster [4, 10, 14, 21].

In a previous study of the synchronization of elliptic bursters, Izhikevich examined a pair of coupled "normal form" elliptic bursters [12] characterized by slow passage through a Bautin (codimension two Andronov–Hopf) bifurcation. In that study, burst (slow activity pattern) synchronization between the bursters was found to be easily achievable, whereas spike (fast activity pattern) synchronization was harder to achieve. Other studies include [7], which examined nonlinearly coupled Bautin bifurcations though not in a bursting setting, and [11, 9, 23, 24], which looked at various aspects of burst and spike synchronization for a variety

*Received by the editors January 8, 2009; accepted for publication (in revised form) by B. Ermentrout December 21, 2009; published electronically March 24, 2010. This work was partially supported by the DAAD/British Council through grant ARC 1286, which funded a visit by the authors to the Mathematical Institute of Cologne University.
http://www.siam.org/journals/siads/9-1/74604.html

†Mathematics Research Institute, School of Engineering, Computing and Mathematics, University of Exeter, Exeter EX4 4QF, UK (aka203@ex.ac.uk, p.ashwin@exeter.ac.uk). The first author's work was partially funded by an Exeter Research Scholarship and by the BBSRC through grant BB/G006369/1.

of coupled burster models.

In this article we study spike synchronization for coupled Bautin-type elliptic bursters with more complicated phase (spiking) dynamics. We show that higher order terms that are not important in the normal form of a single burster can be responsible for nontrivial phase dynamics in coupled bursters even for linear coupling. In particular, we observe and explain coexistence of and transitions between in-phase and antiphase spiking within a single burst for two and more coupled bursters. This sheds light onto possible dynamical patterns of spike synchronization for coupled bursters in neuronal systems in addition to those observed by Sherman [24].

We discuss a normal form for coupled Bautin-type elliptic bursters and focus on burst and spike synchronization in a system of n identical coupled bursters with $z_j \in \mathbb{C}$, $u_j \in \mathbb{R}$, $j = 1, \ldots, n$, given by

$$\left.\begin{aligned} \dot{z}_j &= (u_j + i\omega)\, z_j + B z_j |z_j|^2 + C z_j |z_j|^4 + K_j, \\ \dot{u}_j &= \eta(a - |z_j|)^2, \end{aligned}\right\} \tag{1.1}$$

where $\omega, a, \eta \in \mathbb{R}$ and $B = B_r + iB_i$, $C = C_r + iC_i \in \mathbb{C}$ are fixed parameters and K_j represents coupling. We assume $B_r > 0$ and $C_r < 0$, and set

$$B = 2 + i\zeta = 2 + i\frac{\sigma r_m^2}{2}, \qquad C = -1 + i\gamma = -1 - i\frac{\sigma}{4}. \tag{1.2}$$

We assume that the coupling term is

$$K_j = (\kappa_1 + i\kappa_2) \sum_{k=1}^{n} c_{jk} z_k, \tag{1.3}$$

where $\kappa_1, \kappa_2 \in \mathbb{R}$ are constant coupling parameters and c_{jk} a constant connectivity matrix. For convenience here we take $c_{jk} = 1$ for $j \neq k$, $c_{jj} = 0$, i.e., all-to-all coupling. Biologically, although there are no rigorous reductions of specific bursters to this model, one can think of $z = x + iy$ as comprising a fast variable x that is analogous membrane voltage, y that is analogous to the fast current, and a slow variable u analogous to a slow adaptation current for a neuronal burster.

The article is structured as follows. In section 2 we discuss the individual burster behavior for the model equations (1.1), (1.2), (1.3). In section 2.3 we discuss two coupled bursters ($n = 2$), showing within-burst synchrony changes. These are analyzed in section 3 using a model system with assumed full burst synchrony and slow-fast dynamics [22] to reduce to an equation for within-burst phase difference. Bifurcation analyses of this equation help one understand the observed dynamics of the full model. In section 4.1 we study the effects of noise in the full coupled system and discuss noise-induced bifurcation delays. Furthermore, section 4.2 shows that we can observe similar dynamics in the system with three coupled elliptic bursters, $n = 3$. In section 4.3 we show that within-burst synchrony changes arise in more biologically motivated coupling like gap-junction and nonlinear synaptic coupling, and we conclude with a discussion of some dynamical and biological implications in section 5.

2. The model for coupled Bautin bursters. Bursting is a multiple time scale phenomenon. In bursting, the fast dynamics of repetitive spiking is modulated by a slow dynamics of recurrent alternation between active and quiescent states. As explained in [14], one may obtain bursting from a variety of dynamical mechanisms; here we focus on bursters (1.1)–(1.3) with bursting behavior associated with a Bautin bifurcation. We briefly review the single burster dynamics, and then discuss the spike and burst synchronization for two coupled bursters.

2.1. Normal form for Bautin bifurcation. Suppose we have a Bautin bifurcation, namely, a codimension two Andronov–Hopf bifurcation where the criticality changes on varying an additional parameter. Then there is a normal form that is locally topologically equivalent to the bifurcation, and this normal form may be written [15] for $z = x + iy \in \mathbb{C}$ as

$$\dot{z} = Az + Bz|z|^2 + Cz|z|^4 + O(|z|^6), \tag{2.1}$$

where $A = A_r + iA_i$, B, and C are complex coefficients. One can verify that an Andronov–Hopf bifurcation occurs as A_r passes through 0 and a change of criticality occurs where B_r also passes through zero. The fourth order term is needed to determine the criticality at the degenerate point $B_r = 0$. We write B and C as in (1.2). It can be shown that ζ, γ, and $O(|z|^6)$ terms do not affect the local branching dynamics of the system (2.1). We will, however, argue that ζ and γ may influence the synchrony for two or more coupled elliptic bursters.

From (2.1) we obtain bursting dynamics [11, 12, 14] by coupling the system to a slow variable $u \in \mathbb{R}$ that is the Andronov–Hopf parameter for the Bautin normal form, such that for z small u increases, while for z large u decreases:

$$\left.\begin{aligned} \dot{z} &= (u + i\omega)z + (2 + i\zeta)z|z|^2 + (-1 + i\gamma)z|z|^4, \\ \dot{u} &= \eta(a - |z|^2). \end{aligned}\right\} \tag{2.2}$$

Note that $\eta \ll 1$ is the ratio of the fast to slow time scales. The system (2.2) exhibits bursting for $0 < a < 1$, while tonic spiking sets in for $a > 1$.

In polar form, $z = re^{i\theta}$, (2.2) becomes

$$\left.\begin{aligned} \dot{r} &= ur + 2r^3 - r^5, \\ \dot{\theta} &= \omega + \zeta r^2 + \gamma r^4, \\ \dot{u} &= \eta(a - r^2). \end{aligned}\right\} \tag{2.3}$$

In these coordinates it is clear that the fast subsystem undergoes an Andronov–Hopf bifurcation at $u = 0$ and a limit cycle fold bifurcation (a saddle-node of limit cycles) at $u = -1$. At the saddle-node bifurcation of limit cycles, stable and unstable limit cycles coalesce. A bifurcation sketch for system (2.2) is shown in Figure 1. It is clear from this figure that periodic firing appears at a subcritical Andronov–Hopf bifurcation at $u = 0$ with the emergence of a limit cycle. Likewise the steady state is reached via a saddle-node bifurcation of limit cycles at $u = -1$, where the stable limit cycle (solid line) and the unstable limit cycle (dashed line) meet and eventually cancel each other.

Note that, during bursts, if $\zeta, \gamma \neq 0$, the limit cycles are *nonisochronous;* there is a change in frequency of fast oscillation during the bursts. As this nonisochronicity does not affect the

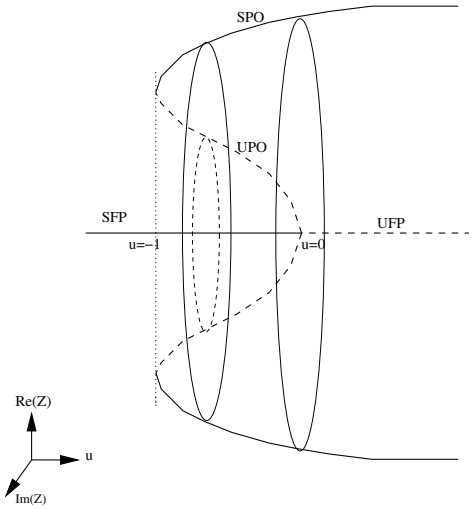

Figure 1. *Schematic bifurcation diagram for z for the fast subsystem of (2.2) on varying u. SFP denotes the stable fixed point, UFP the unstable fixed point, SPO the stable periodic orbit, and UPO the unstable periodic orbit. It is clearly seen that at $u = 0$ the system undergoes subcritical Andronov–Hopf bifurcation, while saddle-node bifurcation of limit cycles occurs at $u = -1$.*

r or u dynamics, or hence the branching behavior, it is not important for single bursters. The phase dynamics in (2.3) depends on amplitude r:

$$\dot{\theta} = \Omega(r) = \omega + \zeta r^2 + \gamma r^4. \tag{2.4}$$

The nontrivial periodic orbits of the system (2.3) are $(r_0, u_0) = (\sqrt{a}, a^2 - 2a)$ for $\eta = 0$. Nontrivial periodic orbits $r \neq 0$ correspond to periodic orbits of (2.2) with periodic spiking. The dynamics of the (2.2) is summarized in Figure 2 for parameters $\omega = 3$, $\eta = 0.1$, $a = 0.8$, $\alpha = 2$, $\beta = -1$, $\zeta = 0$, and $\gamma = 0$. Observe the slow passage effect [3] apparent from Figure 2; although the stability calculation shows that the Andronov–Hopf bifurcation occurs at $u = 0$, simulation shows a delayed bifurcation [3].

Note that we use parameters in (1.2) such that

$$\zeta = \frac{\sigma r_m^2}{2}, \qquad \gamma = -\frac{\sigma}{4}, \tag{2.5}$$

meaning that

$$\frac{d\Omega}{dr} = \sigma r(r_m^2 - r^2). \tag{2.6}$$

From this it is clear that there is a turning point of $\Omega(r)$ at $r = r_m$. The parameter σ can be interpreted as the magnitude of nonisochronicity for the phase dynamics.

2.2. Coupled elliptic bursters. We consider direct linear coupling for the system (2.2) via the fast variables z to give a coupled system of the form (1.1), (1.3) with coupling parameters

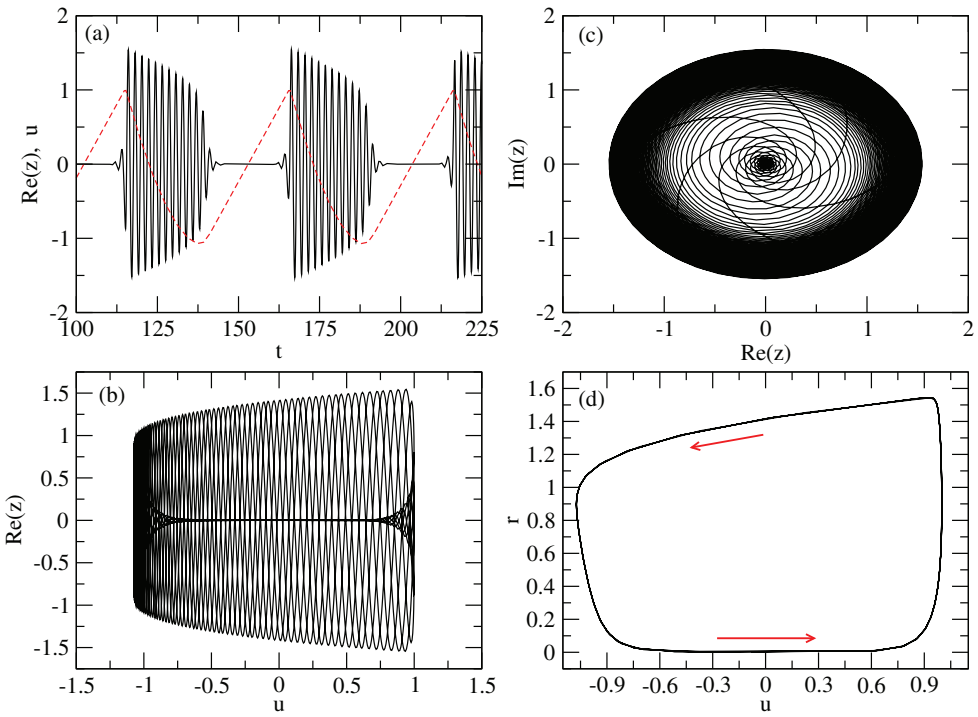

Figure 2. *Dynamics of a single compartment Bautin burster governed by* (2.2) *and* (2.5). *In panel* (a), *the timeseries of* $Re(z)$ *is shown with a solid line, and the corresponding slow variable,* u, *with a dashed line. The parameters for the simulation are* $\omega = 3$, $a = 0.8$, $\eta = 0.1$, $\sigma = 4$, *and* $r_m = 1.35$. *The arrows in* (d) *indicate the direction of change of the slow variable,* u.

κ_1 and κ_2; in section 4.3 we consider other types of coupling. The coefficients c_{jk} for the coupling term of (1.1) are the connectivity matrix; here we assume all-to-all coupling, namely,

$$c_{jk} = \begin{cases} 1 & \text{if } j \neq k, \\ 0 & \text{otherwise.} \end{cases}$$

This form of coupling is analogous to the electrical (gap-junction) coupling between synapses, with phase shift expressed by the argument of $\kappa_1 + i\kappa_2$. Positive κ_1 corresponds to excitatory coupling, while negative κ_1 corresponds to inhibitory coupling.

2.3. Burst and spike synchronization for two coupled bursters. We numerically investigate the dynamics of a pair of coupled elliptic bursters governed by the system (1.1). Burst synchronization between the cells can easily be achieved for a wide range of parameter values with this system. In case of $\kappa_2 = 0$ and $\kappa_1 > 0$ (excitatory coupling), this generally generates in-phase bursts, while antiphase bursts result from inhibitory coupling.[1]

There is a spontaneous within-burst synchrony change observable within Figure 3. The top panel shows x_1 and x_2. All transients were allowed to decay, and the displayed pattern

[1]We write the system (1.1) using $z_1 = x_1 + iy_1$ and $z_2 = x_2 + iy_2$ for the purposes of numerical simulation. All the simulations were done with the interactive package XPPAUT [8]. For integrations, the built-in adaptive Runge–Kutta integrator was used, and results were checked using the adaptive Dormand–Prince integrator.

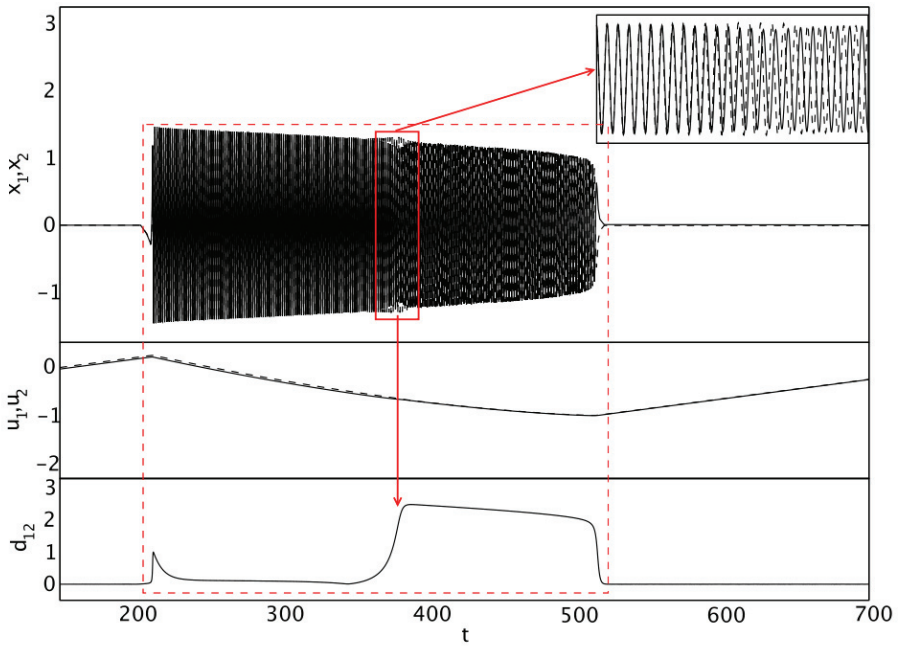

Figure 3. *Within-burst synchrony change from stable in-phase to stable antiphase states for two coupled bursters. The dashed box shows the activity pattern of one burst; the burst repeats periodically, and within-burst synchrony change repeats during each burst. This result is obtained from simulation of* (1.1), (1.2), *and* (1.3) *for* $n = 2$ *and parameters* $\kappa_1 = 0.001$, $\kappa_2 = 0.2$, $\sigma = 3$, $\eta = 0.005$, $r_m = 1.35$, $\omega = 0.01$. *Noise of amplitude* 10^{-5} *was added to the fast subsystem. In this figure, the two coupled bursters are burst synchronized, and the spikes become in-phase at the beginning of the burst but change to antiphase near the middle of the burst. The inset in the topmost panel shows the region of the transition. Note that the initial transient and sudden change in the synchrony pattern along the burst profile are observable from* d_{12}, *where* $d_{12} = 0$ *indicates in-phase synchronization.*

is repeated within each burst. A detail of the middle of the burst is shown in the top-right inset. The corresponding slow variables of the system, u_1 and u_2, are shown in the middle panel. The distinguishing solid and dashed traces correspond to the activity patterns of the two cells, respectively. The bottom panel of the figure shows the Euclidean distance

$$d_{12} = \sqrt{(x_1 - x_2)^2 + (y_1 - y_2)^2 + (u_1 - u_2)^2}$$

between the two systems to show the presence ($d_{12} = 0$) or absence ($d_{12} > 0$) of synchrony. The values of the parameters used in the simulation are $\kappa_1 = 0.001$, $\kappa_2 = 0.2$, $\sigma = 3$, $\eta = 0.005$, $r_m = 1.35$, $\omega = 0.01$. Wiener noise of amplitude 10^{-5} was added to the fast variables (see section 4.1 for a discussion of the effect of noise).

The spikes are in-phase at the beginning of the burst, but change to antiphase within the burst. The inset shows the region of this transition. This transition region may be shifted along the burst profile by changing r_m. Larger values of r_m shift this transition towards

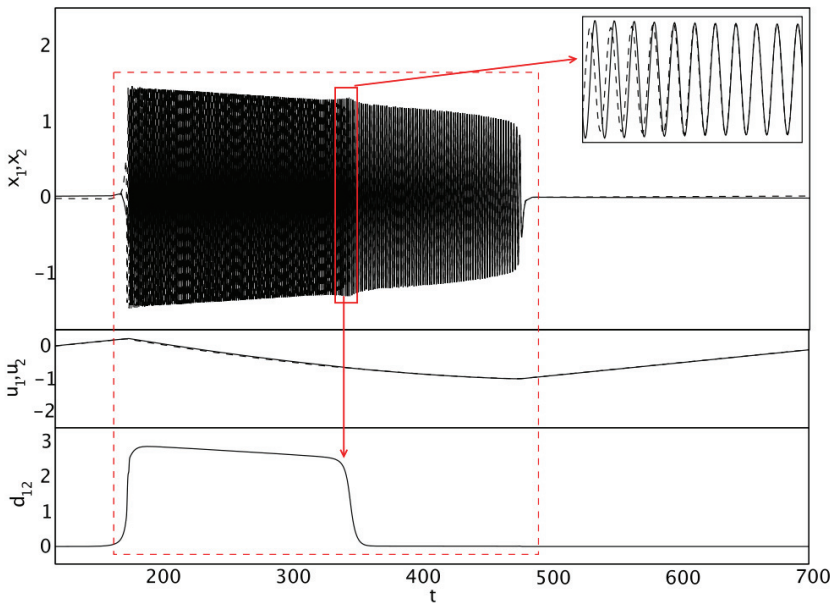

Figure 4. *Within-burst synchrony change from stable antiphase to stable in-phase states. The governing system and details as in Figure 3 except* $\kappa_2 = -0.2$. *The inset in the topmost panel shows the transition in detail. In the last panel, the bump in* d_{12} *signifies the antiphase synchronization of the spikes within the synchronized burst. The corresponding slowly changing variables,* u_1 *and* u_2, *are shown in the middle panel with solid and dotted lines, respectively.*

the beginning of the burst with larger amplitude spikes, and vice versa. This change in the synchrony pattern along the burst profile is also captured by d_{12}.

We present another example of within-burst synchrony change for different parameter values in Figure 4, where spikes of the two coupled cells start antiphase and change to in-phase during the burst. As before, low amplitude noise of order 10^{-5} was added to fast variables. The inset in the first panel shows the region of the transition. In the last panel, d_{12} indicates that the burst is initially antiphase, and as it returns to $d_{12} = 0$ there is a transition to in-phase synchronization of the within-burst spikes of the two cells. The corresponding slowly changing current variables, u_1 and u_2, are shown in the middle panel. The overlapped solid and dashed lines imply the in-phase burst synchronization of the coupled system.

3. A burst synchronized constrained model. Although it is possible to find within-burst synchrony changes within (1.1), (1.2), (1.3), it is hard to explain their existence analytically from the full model. To overcome this, we reduce the coupled system to a constrained problem where we assume burst synchronization, followed by a slow-fast decomposition. Using this simplified model, we can explain how nonisochronicity and linear coupling can lead to within-burst synchrony changes.

3.1. Two coupled bursters in polar coordinates. Writing (1.1), (1.2), (1.3) in polar coordinates, $z_j = r_j e^{i\theta_j}$ for $n = 2$ gives the system

$$
\left.\begin{aligned}
\dot{r}_1 &= u_1 r_1 + 2r_1^3 - r_1^5 + r_2(\kappa_1 \cos(\theta_2 - \theta_1) - \kappa_2 \sin(\theta_2 - \theta_1)),\\
\dot{\theta}_1 &= \omega + \frac{1}{2}\sigma r_m^2 r_1^2 - \frac{1}{4}\sigma r_1^4 + \frac{r_2}{r_1}(\kappa_1 \sin(\theta_2 - \theta_1) + \kappa_2 \cos(\theta_2 - \theta_1)),\\
\dot{u}_1 &= \eta(a - r_1^2),\\
\dot{r}_2 &= u_2 r_2 + 2r_2^3 - r_2^5 + r_1(\kappa_1 \cos(\theta_1 - \theta_2) - \kappa_2 \sin(\theta_1 - \theta_2)),\\
\dot{\theta}_2 &= \omega + \frac{1}{2}\sigma r_m^2 r_2^2 - \frac{1}{4}\sigma r_2^4 + \frac{r_1}{r_2}(\kappa_1 \sin(\theta_1 - \theta_2) + \kappa_2 \cos(\theta_1 - \theta_2)),\\
\dot{u}_2 &= \eta(a - r_2^2).
\end{aligned}\right\} \tag{3.1}
$$

We constrain the system to exact burst synchronization by replacing the equations for $\dot{u}_1$ and $\dot{u}_2$ by

$$
\left.\begin{aligned}
u(t) &= u_1(t) = u_2(t),\\
\dot{u} &= \dot{u}_1 = \dot{u}_2 = \eta\left(a - \frac{1}{2}(|z_1|^2 + |z_2|^2)\right).
\end{aligned}\right\} \tag{3.2}
$$

Thus, the system (3.1) may be written with constraint (3.2) and $\phi = \theta_1 - \theta_2$ as

$$
\left.\begin{aligned}
\dot{r}_1 &= u r_1 + 2r_1^3 - r_1^5 + \kappa_1 r_2 \cos\phi + \kappa_2 r_2 \sin\phi,\\
\dot{r}_2 &= u r_2 + 2r_2^3 - r_2^5 + \kappa_1 r_1 \cos\phi - \kappa_2 r_1 \sin\phi,\\
\dot{\phi} &= \frac{1}{2}\sigma r_m^2 (r_1^2 - r_2^2) - \frac{1}{4}\sigma(r_1^4 - r_2^4)\\
&\quad - \kappa_1\left(\frac{r_1^2 + r_2^2}{r_1 r_2}\right)\sin\phi - \kappa_2\left(\frac{r_1^2 - r_2^2}{r_1 r_2}\right)\cos\phi,\\
\dot{u} &= \eta\left(a - \frac{1}{2}(r_1^2 + r_2^2)\right).
\end{aligned}\right\} \tag{3.3}
$$

As we are interested in synchrony changes, we define longitudinal and transverse coordinates:

$$
\left.\begin{aligned}
r_l &= \frac{r_1 + r_2}{2},\\
r_t &= \frac{r_1 - r_2}{2}.
\end{aligned}\right\} \tag{3.4}
$$

The system (3.1) reduces to the four-dimensional system

$$
\left.\begin{aligned}
\dot{r}_l &= u r_l + 2r_l^3 + 6r_l r_t^2 - r_l^5 - 10r_l^3 r_t^2 - 5r_l r_t^4\\
&\quad + \kappa_1 r_l \cos\phi - \kappa_2 r_t \sin\phi,\\
\dot{r}_t &= u r_t + 6r_l^2 r_t + 2r_t^3 - 5r_l^4 r_t - 10r_l^2 r_t^3 - r_t^5\\
&\quad - \kappa_1 r_t \cos\phi + \kappa_2 r_l \sin\phi,\\
\dot{\phi} &= 2\sigma r_m^2 r_l r_t - 2\sigma r_l r_t (r_l^2 + r_t^2)\\
&\quad - 2\kappa_1 \frac{(r_l^2 + r_t^2)}{r_l^2 - r_t^2}\sin\phi - 4\kappa_2 \frac{r_l r_t}{r_l^2 - r_t^2}\cos\phi,\\
\dot{u} &= \eta(a - (r_l^2 + r_t^2)).
\end{aligned}\right\} \tag{3.5}
$$

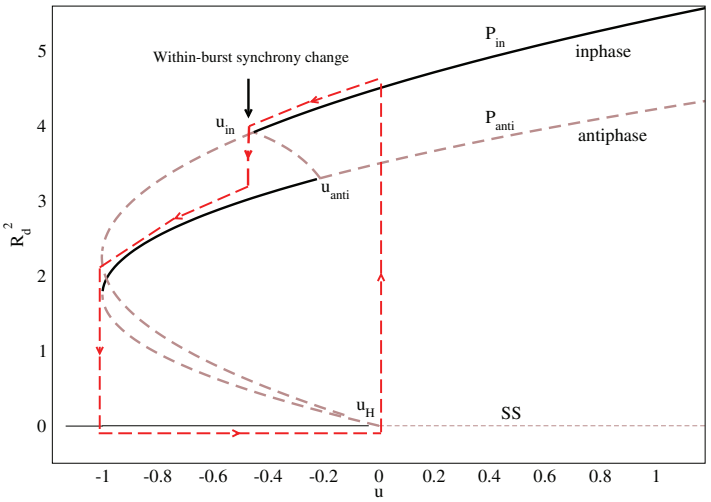

Figure 5. *Bifurcation of the fast dynamics for the coupled constrained system (3.3), plotting R_d^2 against u (see (3.6)) and with parameters as in Figure 3. The branches P_{in} and P_{anti} are the in-phase and antiphase periodic branches of the system. The steady-state branch is denoted by SS. Solid and dashed parts of the branches denote the stable and unstable solutions, respectively. u_{in} and u_{anti} denote locations of bifurcations giving loss of stability of the in-phase and antiphase periodic orbits, respectively, while u_H is the Andronov–Hopf bifurcation of SS. The dashed loop indicates how the slow dynamics generates periodic bursts. Note that the switching of the trajectory from in-phase to antiphase along the periodic branches implies a within-burst synchrony change.*

Here, (r_l, r_t, ϕ) govern the fast dynamics, and u governs the slow dynamics. The system (3.5) is a reduced four-dimensional realization of the full system (3.1) for a pair of coupled elliptic bursters. Figure 5 shows a bifurcation diagram for the fast subsystem of (3.3) on varying u. The dashed loop indicates how a periodic burst including a within-burst synchrony change can occur: we define an observable R_d^2 by

$$R_d^2 = r_1^2 + r_2^2 + \frac{1}{4} r_1 r_2 \cos\phi. \tag{3.6}$$

Note that R_d is such that $R_d = \frac{9}{4}r$ if the oscillations are in-phase and $R_d = \frac{7}{4}r$ if they are antiphase, and $r_1 = r_2 = r$. Note also that R_d is symmetric under interchange of the bursters.

In [24] antiphase, asymmetric, or quasi-periodic spike synchrony patterns were reported from a system of two gap-junction-coupled pancreatic β-cells. The authors attributed this to bifurcations of the periodic branches of the fast subsystem for a similarly burst constrained system. They showed numerically that as coupling strength increases, the spikes of the coupled cell pairs change from antiphase to in-phase through a regime of quasi-periodic and asymmetric periodic oscillations. The antiphase branch was found to arise as a secondary Andronov–Hopf bifurcation from the steady-state, the asymmetric periodic branch as a pitchfork bifurcation from the in-phase state, and the quasi-periodic state as a torus bifurcation from the antiphase branch. The author of [24] did not observe multistability of spike synchrony states or synchrony changes between the in-phase oscillations and antiphase oscillations within a burst period. By contrast, Figure 5 shows that the bursting system (1.1), (1.2), (1.3) may have both stable in-phase and antiphase branches within a burst period and spikes that go

spontaneously from in-phase to antiphase via a pitchfork bifurcation on the in-phase periodic branch.

3.2. Stability analysis of the burst constrained system. In this section, we carry out a linear stability analysis of the fast subsystem of (3.5) about in-phase and antiphase states with $r_t = 0$ and $r_l = r$, which means both cells are burst synchronized and $r_1 = r_2 = r$. In the analysis, we assume that the slow variable u is a constant of the system by setting the time scale ratio, $\eta = 0$, as a singularly perturbed parameter. The dynamics, as a result, is governed only by the fast spiking activity. For $r_t = 0$ and $\eta = 0$ we write $r_l = r$ as the stable nontrivial solution of (3.5) in the appropriate subspace,

$$\dot{r}_l = (u + 2\kappa_1 \cos\phi) r_l + 2r_l^3 - r_l^5, \tag{3.7}$$

corresponding to bursting behavior. Note that for small $|\kappa_1|$ this will have a solution close to that of the single burster case.

If we consider the fast subsystem of (3.5) with u between -1 and $+1$, then we can verify the existence of two solutions:

- in-phase, where $r_t = \phi = 0$, $r_l = r$,
- antiphase, where $r_t = 0$, $\phi = \pi$, $r_l = r$,

where $r > 0$ is a solution of

$$u = r^4 - 2r^2 - 2\kappa_1 \cos\phi. \tag{3.8}$$

The Jacobian for the fast subsystem at the in-phase solution is block diagonal with one single real eigenvalue and a block

$$J_{in} = \begin{pmatrix} u + 6r^2 - 5r^4 - \kappa_1 & \kappa_2 r \\ 2\sigma r_m^2 r - 2\sigma r^3 - \frac{4\kappa_2}{r} & -2\kappa_1 \end{pmatrix}. \tag{3.9}$$

Likewise, the Jacobian for the fast system at the antiphase solution is also block diagonal with a single real eigenvalue and a block

$$J_{anti} = \begin{pmatrix} u + 6r^2 - 5r^4 + \kappa_1 & -\kappa_2 r \\ 2\sigma r_m^2 r - 2\sigma r^3 + \frac{4\kappa_2}{r} & 2\kappa_1 \end{pmatrix}. \tag{3.10}$$

Note that the off-diagonal entries of the Jacobian matrices (3.9) and (3.10) depend on the imaginary part of the coupling coefficient, κ_2, and other system parameters. The real eigenvalues can be assumed negative because of stability of the solution of (3.7).

The eigenvalues of (3.9) can be determined by examining the trace

$$\mathrm{tr}(J_{in}) = u + 6r^2 - 5r^4 - 3\kappa_1 \tag{3.11}$$

and the determinant

$$\det(J_{in}) = -2(u + 6r^2 - 5r^4)\kappa_1 - 2\sigma r^2 (r_m^2 - r^2)\kappa_2 + 2\kappa_1^2 + 4\kappa_2^2. \tag{3.12}$$

Similarly, we can understand their antiphase counterparts from (3.10) by examining

$$\mathrm{tr}(J_{anti}) = u + 6r^2 - 5r^4 + 3\kappa_1 \tag{3.13}$$

and

$$\det(J_{anti}) = 2(u + 6r^2 - 5r^4)\kappa_1 + 2\sigma r^2(r_m^2 - r^2)\kappa_2 + 2\kappa_1^2 + 4\kappa_2^2. \tag{3.14}$$

For simplicity, we consider a special case when $\kappa_1 = 0$ and $|\kappa_2| \ll 1$. In such a case, it may easily be seen that both $\mathrm{tr}(J_{in})$ and $\mathrm{tr}(J_{anti})$ in (3.11) and (3.13), respectively, are negative, as stability of the periodic solution of (3.7) means that $u + 6r^2 - 5r^4 < 0$. So, from (3.11) and (3.13), $\mathrm{tr}(J_{in}) < 0$, and $\mathrm{tr}(J_{anti}) < 0$. For this weak coupling, it is also evident that $(\mathrm{tr}(J_{in(anti)}))^2 > 4\det(J_{in(anti)})$. Hence, the system will have a stable node for $\det(J_{in(anti)}) > 0$ and a saddle for $\det(J_{in(anti)}) < 0$.

To explain the within-burst synchrony change observed in Figures 3 and 4, we write (3.12) and (3.14) to first order in κ_2, approximate $\kappa_1 = 0$, and consider small $\kappa_2 > 0$, obtaining

$$\det(J_{in}) = -2\sigma r^2(r_m^2 - r^2)\kappa_2 + O(\kappa_2^2) \tag{3.15}$$

and

$$\det(J_{anti}) = 2\sigma r^2(r_m^2 - r^2)\kappa_2 + O(\kappa_2^2). \tag{3.16}$$

From (3.15), if $r > r_m + O(\kappa_2)$, then $\det(J_{in}) > 0$. Together with the condition $\mathrm{tr}(J_{in}) < 0$, this implies that the in-phase solution is stable, whereas (3.16) implies that the antiphase solution is unstable for $r < r_m + O(\kappa_2)$. We may derive approximate expressions for $r(= r_l)$ where the bifurcations take place. We denote the bifurcation value for amplitude of the in-phase solution by r_{in}, and the amplitude of the antiphase solution by r_{anti}. Note that r_{in} may be obtained by equating $\det(J_{in})$ to zero in (3.12) with $\kappa_1 = 0$, giving

$$\det(J_{in}) = -\kappa_2(2\sigma r_{in}^2 - 2\sigma r_{in}^2 r_m^2 - 4\kappa_2) = 0. \tag{3.17}$$

Now solving (3.17) gives

$$r_{in} = r_m\left(1 - \frac{\kappa_2}{\sigma r_m^4}\right) + O(\kappa_2^2). \tag{3.18}$$

Likewise, from (3.14), the bifurcation point, r_{anti}, may be obtained as

$$r_{anti} = r_m\left(1 + \frac{\kappa_2}{\sigma r_m^4}\right) + O(\kappa_2^2). \tag{3.19}$$

Note that r depends on u via (3.8). So, the corresponding bifurcation points for in(anti)phase oscillations can be derived from (3.18), (3.19), and (3.8) for the special case $\kappa_1 = 0$ as

$$u_{in} = r_m^2(r_m^2 - 2) + \frac{4\kappa_2}{\sigma r_m^2}(1 - r_m^2) + O(\kappa_2^2) \tag{3.20}$$

and

$$u_{anti} = r_m^2(r_m^2 - 2) - \frac{4\kappa_2}{\sigma r_m^2}(1 - r_m^2) + O(\kappa_2^2). \tag{3.21}$$

Note that a more general analysis of these bifurcation points for nonzero κ_1 and κ_2 can be undertaken by examining the roots of (3.12), (3.14).

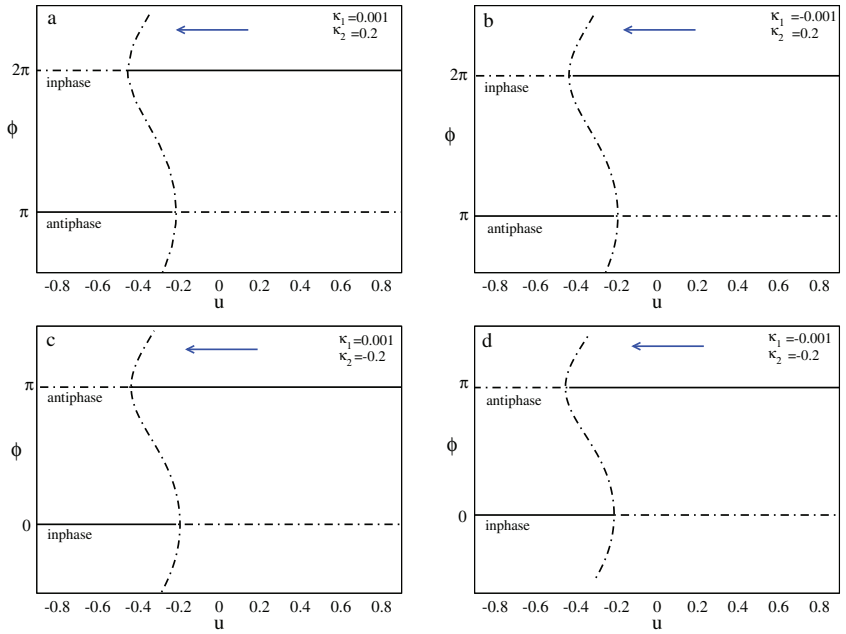

Figure 6. *Bifurcation diagram of ϕ against u for the burst synchronized constrained system (3.3), where u is a parameter that slowly decreases during each burst, as shown by the arrow. The parameters are $\omega = 3$, $\sigma = 3$, $r_m = 1.35$, and different κ_1 and κ_2 as indicated in the panels from* (a) *to* (d). *Note that* (a) *corresponds to the parameters in Figure 3 and 5 and* (c) *to that in Figure 4. The solid lines represent stable solutions, while the unstable solutions are shown with dash-dotted lines.*

3.3. Synchrony bifurcations of the fast subsystem. We now extend the numerical bifurcation analyses of the fast subsystem (3.3) from Figure 5 by taking η as the singular perturbation parameter to take the fast system through single bursts and to compare with the asymptotic results found for $\kappa_1 = 0$.

In Figure 6 we present bifurcations of bursting solutions of (3.3) projected onto the phase difference, ϕ, as u is varied. The solid line represents the stable periodic solutions, while the unstable solutions are shown with dash-dotted lines. The arrow, running from right to left, shows the direction of the change of u. Figure 6(a) shows a burst that begins with a stable in-phase solution; until almost halfway through the burst, the in-phase solution remains stable, and then the antiphase solutions gain stability. The coupling coefficients in these results are $\kappa_1 = 0.001$ and $\kappa_2 = 0.2$. The other parameter values are $\sigma = 3$, $\omega = 3$, and $r_m = 1.35$. This behavior agrees with the simulation result shown in Figures 3 and 5, both obtained for the same parameters. Similarly, Figure 6(c) explains what is found in the simulation in Figure 4. Here, the burst starts off in stable antiphase and changes to stable in-phase. Figure 6(b) and (d) show the results with $\kappa_1 = -0.001$ but different κ_2. An interesting observation is the presence of the bistable region around the middle of the burst separating the stable in-phase and antiphase solutions. This region occurs near the transition point ($r_m = 1.35$) along the burst profile, as predicted in the analysis in the previous section. These bifurcations show the robust coexistence of the in-phase and antiphase synchrony patterns of the within-burst spikes for a range of u, and within-burst synchrony changes of the coupled bursting system

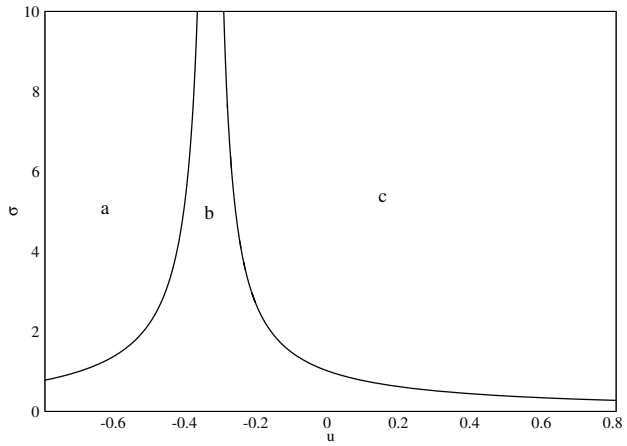

Figure 7. *Two-parameter bifurcation diagram of σ against u for the fast subsystem of (3.3). The other parameters are fixed at $\kappa_1 = 0.001$, $\kappa_2 = 0.2$, and $r_m = 1.35$. There are stable in-phase oscillations in regions* b *and* c*, and stable antiphase oscillations in regions* a *and* b.

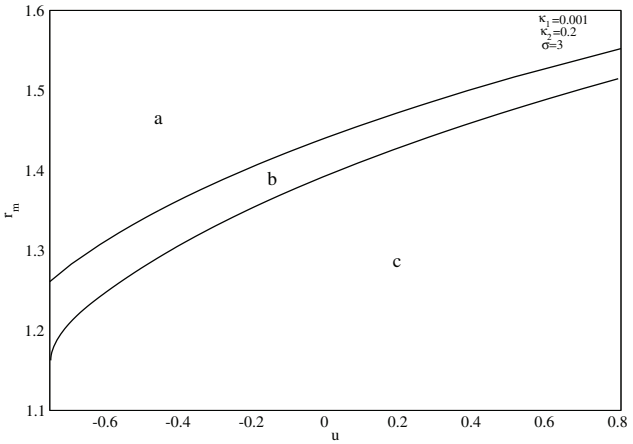

Figure 8. *Two-parameter bifurcation diagram of r_m against u for system and parameters as in Figure 7 and $\sigma = 3$. There are stable in-phase oscillations in regions* b *and* c*, and stable antiphase oscillations in regions* a *and* b.

(1.1).

Figure 7 shows a two-parameter bifurcation diagram in the $u\sigma$ plane. As σ increases, the bistable region is seen to get narrower, in agreement with (3.18) and (3.19). Likewise, Figure 8 is obtained from the parameters $\kappa_1 = 0.001$, $\kappa_2 = 0.2$, and $\sigma = 3$. This figure shows how the position of the bistable region b changes on varying r_m.

The role of the coupling parameter κ_1 is shown in Figures 9 and 10 for two values of κ_2. The parameters in Figure 9 are $\kappa_2 = 0.2$, $\sigma = 3$, and $r_m = 1.35$, and the behavior is similar to that in Figure 6(a) and (b). It is interesting to note that within-burst synchrony changes appear even for weak inhibitory coupling ($\kappa_1 < 0$). Moreover, stronger inhibitory values of κ_1 would mean only antiphase spike synchronization. Similarly, Figure 10 demonstrates dynamics similar to those of Figure 6(c) and (d). Figure 10 has the same parameters as

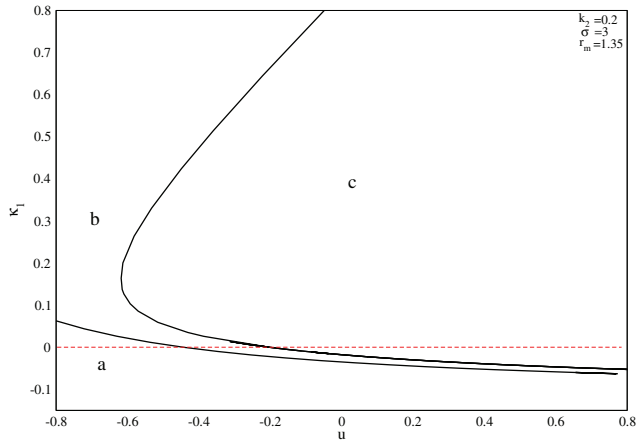

Figure 9. *Bifurcation diagram of* κ_1 *against* u *for system and parameters as in Figure* 6(a),(b) *with* $\kappa_2 = 0.2$. *There are stable in-phase oscillations in regions* b *and* c, *and stable antiphase oscillations in regions* a *and* b.

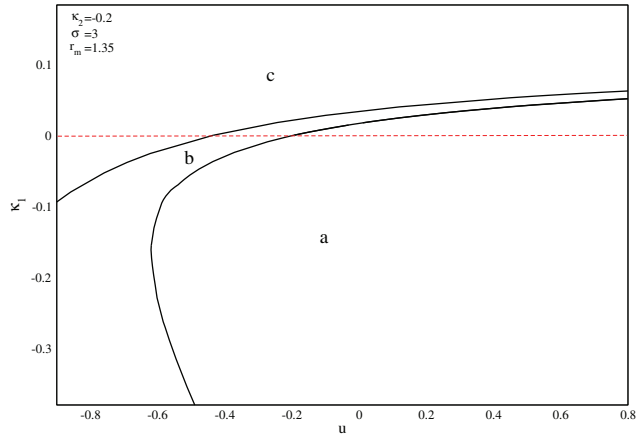

Figure 10. *Two-parameter bifurcation diagram of* κ_1 *against* u *for system and parameters as in Figure* 6(c),(d) *with* $\kappa_2 = -0.2$. *There are stable antiphase oscillations in regions* a *and* b, *and stable in-phase oscillations in regions* b *and* c.

those in Figure 9 except $\kappa_2 = -0.2$. The excursion of the bistable region b above the dotted horizontal line indicates the appearance of within-burst synchrony changes for weak excitatory values, $\kappa_1 > 0$. Stronger κ_1 results in in-phase spike synchronization.

Tables 1 and 2 show the comparison of the in-phase and antiphase bifurcation points, r_{in}, u_{in} and r_{anti}, u_{anti}, for $\kappa_1 = 0$ and two values of κ_2 calculated from (3.18), (3.20) and (3.19), (3.21), respectively, with those from simulations of systems (3.3). Note that the bifurcation points obtained from (3.3) and the approximations of (3.18), (3.19), (3.20), (3.21) agree very well.

Figures 11 and 12 portray bifurcation diagrams in $u\kappa_2$-space for two values κ_1. These figures show the role of κ_2 in spike synchronization. Figure 11 uses the parameters $\kappa_1 = 0.001$, $\sigma = 3$, $r_m = 1.35$. For negative and weak positive values of κ_2 (region c) only stable in-phase

Table 1

Comparison of the bifurcation points, r_{in}, r_{anti}, u_{in}, and u_{anti}, obtained from simulations of system (3.3) and those from (3.18), (3.19), (3.20), (3.21) for $\kappa_1 = 0$, $\kappa_2 = 0.2$, $\sigma = 3$, and $r_m = 1.35$.

	r_{in}	r_{anti}	u_{in}	u_{anti}
From system (3.3) (Figure 9)	1.3210	1.376	−0.4433	−0.2027
From (3.18), (3.19), (3.20), (3.21)	1.3229	1.3771	−0.4438	−0.2032

Table 2

Comparison of the bifurcation points as in Table 1, except $\kappa_2 = -0.2$.

	r_{in}	r_{anti}	u_{in}	u_{anti}
From system (3.3) (Figure 10)	1.376	1.321	−0.2027	−0.4433
From (3.18), (3.19), (3.20), (3.21)	1.377	1.3229	−0.2032	−0.4438

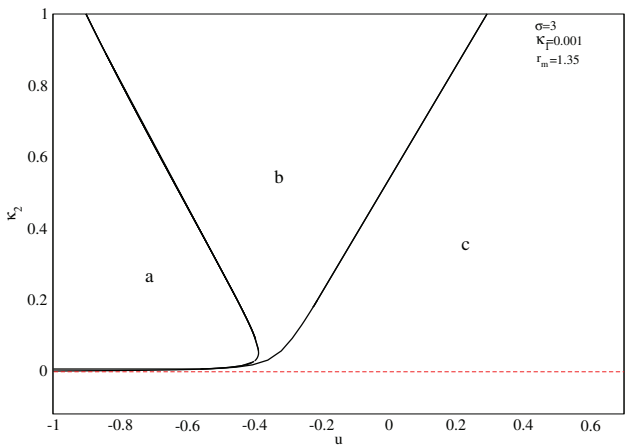

Figure 11. *Two-parameter bifurcation diagram of κ_2 against u for system and parameters as in Figure 6(a),(b) with $\kappa_1 = 0.001$. There are stable in-phase oscillations in regions* b *and* c*, and stable antiphase oscillations in regions* a *and* b.

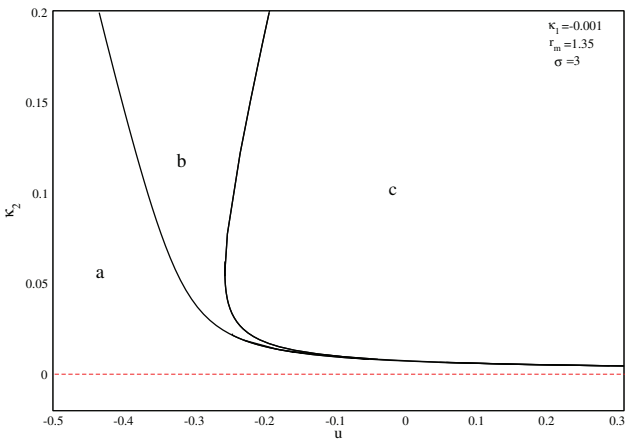

Figure 12. *Bifurcation diagram as in Figure 11, but with $\kappa_1 = -0.001$. There are stable in-phase oscillations in regions* b *and* c*, and stable antiphase oscillations in regions* a *and* b.

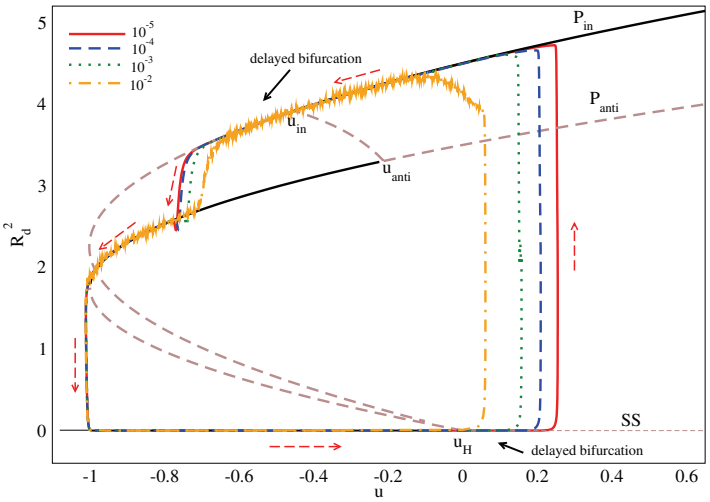

Figure 13. *Noise dependent bifurcation delays at both onset of burst from Andronov–Hopf bifurcation point at u_H and within-burst synchrony change at u_{in} for two coupled bursters (1.1), (1.2), (1.3). The trajectories for the four indicated amplitudes of added noise (with same initial conditions and parameters as in Figure 3 with $u = \frac{u_1+u_2}{2}$) are superimposed on the bifurcation diagram of Figure 5. The dashed arrows show the direction of trajectory during a periodic burst. Note that the delays reduce with increasing noise amplitude; this is a typical slow passage effect.*

solutions are present. Figure 12 shows the bifurcation diagram for $\kappa_1 = -0.001$. As before, a and b are regions of stable antiphase, and b and c the stable in-phase oscillations. It may be observed that for negative and weak positive values of κ_2 (region a), one can see only stable antiphase synchronization of spikes in the burst.

4. Understanding within-burst synchrony changes from the constrained system. Recall from Figure 5 that the constrained system can be used to explain periodic bursting with a within-burst synchrony change in coupled bursters. In this section we examine the effect of noise and the extension to three bursters and to more general couplings.

4.1. Effects of noise on within-burst synchrony changes. We include in this section a brief discussion of the influence of noise on the phenomenon of within-burst synchrony changes for coupled elliptic bursters. It is well known that bursters are significantly affected by the presence of noise, even if it is low amplitude, because of slow passage effects. In particular, the Andronov–Hopf bifurcation at the onset of each burst is delayed by a time approximately proportional to the logarithm of the noise level [25, 3, 17, 18]. This effect can be understood as a delay in leaving the neighborhood of the quiescent equilibrium state after it has gone unstable (i.e., where the slow variable passes through the Andronov–Hopf bifurcation point shown in Figure 2(d)); larger amplitude noise generates the required fluctuation sooner.

However, there is an additional effect: within-burst synchrony change also exhibits a slow passage effect (a delayed pitchfork bifurcation at loss of synchrony). Figure 13 exhibits evidence of both slow passage effects; there are delays corresponding to transitions to bursting and synchrony change (u_H and u_{in}, respectively), depending on noise amplitude. On increasing noise above 10^{-2} (not shown), the synchrony change is no longer apparent because there

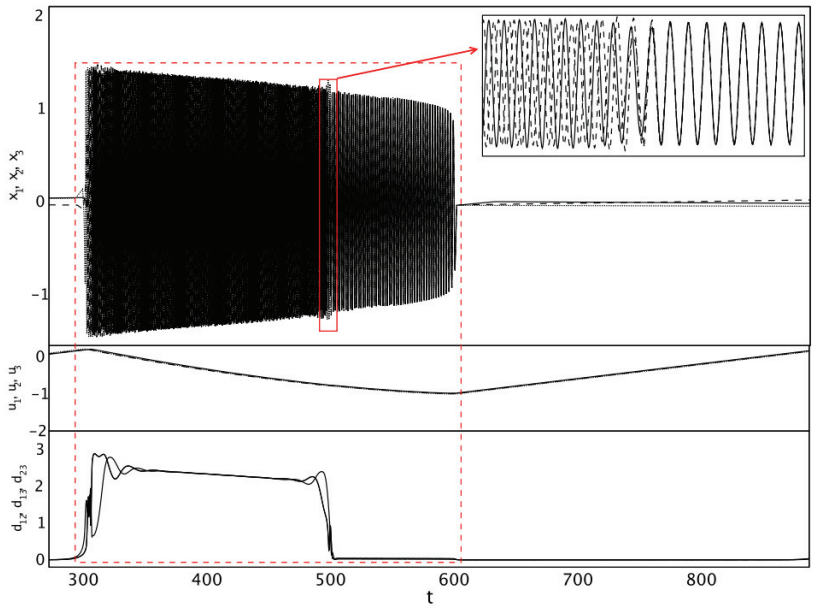

Figure 14. *Within-burst synchrony change from stable antiphase to stable in-phase states for three coupled Bautin-type elliptic bursters; see text for details. All three cells burst synchronously, but the fast spikes are antiphase at the beginning and in-phase by the end of the burst.*

are large fluctuations in the amplitude and phase difference within burst caused by the noise. Moreover, if the noise level is too small, the delay to the within-burst synchrony change may become longer than the length of the burst. Indeed, the system without noise may become "stuck" in an in-phase solution for the whole burst.

4.2. Burst and spike synchronization for three bursters. We briefly demonstrate that within-burst synchrony changes are present in larger numbers of coupled bursters. In particular we look at three coupled Bautin-type elliptic bursters, i.e., (1.1), (1.2), and (1.3) with $n = 3$. A simulation of this system is shown in Figure 14 with parameters $\omega = 0.1$, $r_m = 1.35$, $\sigma = 5$, $\kappa_1 = -0.001$, $\kappa_2 = -0.2$, and additive noise of amplitude 10^{-5} to the fast variables.

The figure shows behavior very similar to that of the two-burster system, with the difference that the antiphase state is where the three bursters have a phase shift of $\frac{2\pi}{3}$ relative to each other. The oscillations at the beginning of the burst are antiphase in this sense, and there is a transition to in-phase during the burst. The inset in the top panel of the figure shows the transition in the spike synchrony pattern during the burst. The activity of the three different bursters is shown in solid, dashed, and dash-dotted lines. The middle panel shows evolution of the corresponding slow variables, $u_1(t)$, $u_2(t)$, and $u_3(t)$. The third panel plots d_{12}, d_{13}, and d_{23} that all must be zero for in-phase synchronization, where

$$d_{ij} = \sqrt{(x_i - x_j)^2 + (y_i - y_j)^2 + (u_i - u_j)^2},$$

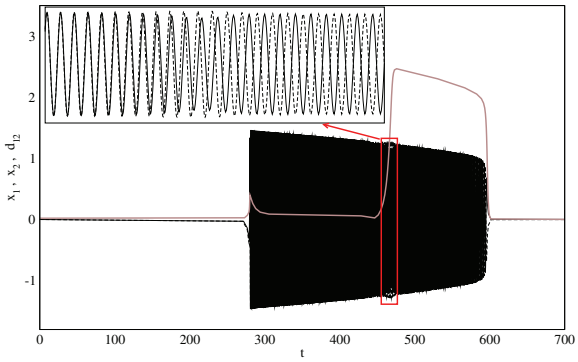

Figure 15. *Within-burst synchrony change from stable in-phase to stable antiphase states for two coupled bursters governed by the system (1.1), (1.2) and gap-junction coupling (4.1). This pattern repeats during each burst. The parameters are* $\sigma = 5$, $\kappa_1 = -0.001$, $\kappa_2 = 0.2$, $r_m = 1.35$, $\omega = 0.001$, *and* $\eta = 0.005$. *A low amplitude noise of order* 10^{-6} *is added to the components of the fast subsystem.*

with $i, j = 1, 2, 3$.

4.3. Examples with biologically motivated coupling. We now demonstrate that within-burst synchrony changes may also emerge in systems of coupled Bautin bursters with more biologically motivated coupling schemes: this includes gap-junction coupling, i.e., a linear diffusive coupling, and nonlinear synaptic coupling as discussed in [7, 23] in the context of the Bautin normal form. First, we consider gap-junction coupling K_j in (1.1) as

$$K_j = (\kappa_1 + i\kappa_2) \sum_{k=1}^{n} c_{jk}(z_k - z_j), \tag{4.1}$$

with $j \neq k$ but still a complex coefficient as in [7, 23]. Figure 15 demonstrates a simulation of (1.1), (1.2) for two coupled Bautin bursters with gap-junction coupling (4.1). It is apparent from this figure that the system undergoes within-burst synchrony changes from in-phase to antiphase. Second, we consider cubic coupling between the bursters as an approximation to nonlinear synaptic coupling [7]:

$$K_j = (\kappa_1 + i\kappa_2) \sum_{k=1}^{n} c_{jk} z_k^2 \bar{z}_k. \tag{4.2}$$

Figure 16 shows the simulation of (1.1), (1.2) with nonlinear coupling (4.2) for two coupled bursters. As in the direct and gap-junction coupling cases, the system undergoes within-burst synchrony changes from in-phase to antiphase. We have not done a detailed analysis of burst constrained systems with gap-junction and nonlinear synaptic coupling, but this should be possible as in section 3. The simulations presented here show in particular that direct coupling is not necessary for within-burst synchrony changes in coupled Bautin bursters.

5. Conclusion. We study the spiking dynamics of coupled elliptic bursters and find that repeated within-burst synchrony changes are possible even for a simple normal form model, as long as terms that break isochronicity of the normal form are included. We observe that

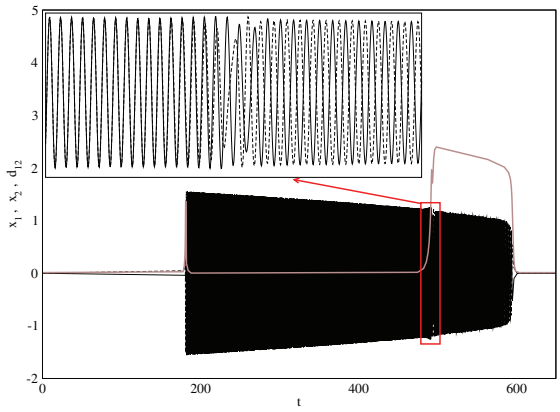

Figure 16. *Within-burst synchrony change from stable in-phase to stable antiphase states for two coupled bursters governed by the system* (1.1), (1.2) *and nonlinear synaptic coupling* (4.2). *This pattern repeats during each burst. The parameters are* $\sigma = 5$, $\kappa_1 = -0.001$, $\kappa_2 = 0.2$, $r_m = 1.35$, $\omega = 0.003$, *and* $\eta = 0.005$.

within-burst synchrony changes are stable and robust to changes in parameters. However, for identical bursters these within-burst changes are robust and therefore easy to observe in the presence of noise. Moreover, Figure 13 shows that increasing noise reduces the slow passage effect of both bifurcation points, i.e., the onset of bursting and the within-burst synchrony changes.

By reduction to fast-slow dynamics for the constrained burst synchronized model, we analyze the appearance of the within-burst synchrony change for two oscillators, and the influence of various system parameters. In particular we find that a turning point in the frequency Ω can be associated with the observed within-burst synchrony changes, analogous to bifurcations observed in systems of coupled weakly dissipative oscillators [2]. Moreover, we can find the approximate location of the transition between stable in-phase and antiphase oscillations from bifurcation analysis of a reduced system.

The examples we have illustrated in this paper are clearest for long bursts where there are many oscillations within a burst. Similar effects are also present in shorter bursts, but are harder to observe because the changes in synchrony must occur over a small number of spikes to be observable. Moreover, burst length is inversely proportional to the slow time scale η, so the clearest within-burst synchrony changes are observed for sufficiently small η. Also note that eigenvalues for the fast subsystem (3.9), (3.10) depend on the coupling strength but not on η, so apart from bifurcation delay, we expect no constraint between η, κ_1, and κ_2 other than all being small enough.

For larger populations of oscillators we expect there can be not just transitions between in-phase and antiphase during bursts, but also spontaneous changes in clustering, leading to robust but sensitive phase dynamics [1, 20], and we believe that this study gives some insight into the range of synchrony dynamics of coupled bursters in general. In particular, section 4 shows that direct coupling is not necessary for within-burst synchrony changes. Better understanding of spike synchronization in more general coupled burster networks may lead to better understanding of potentially important new mechanisms for information processing and transmission by coupled neuronal bursters. This is discussed, for example, in [13], where it

is suggested that information transmission may occur via resonance between burst frequency and subthreshold oscillations.

Acknowledgments. The authors would like to thank Svitlana Popovych for her useful comments on the research. They would also like to thank the anonymous referees for useful and detailed comments.

REFERENCES

[1] P. Ashwin and J. Borresen, *Encoding via conjugate symmetries of slow oscillations for globally coupled oscillators*, Phys. Rev. E (3), 70 (2004), paper 026203.
[2] P. Ashwin and G. Dangelmayr, *Reduced dynamics and symmetric solutions for globally coupled weakly dissipative oscillators*, Dyn. Syst., 20 (2005), pp. 333–367.
[3] S. M. Baer, T. Erneux, and J. Rinzel, *The slow passage through a Hopf bifurcation: Delay, memory effects, and resonance*, SIAM J. Appl. Math., 49 (1989), pp. 55–71.
[4] S. Coombes and P. C. Bressloff, eds., *Bursting, The Genesis of Rhythm in the Nervous System*, World Scientific Publishing, Hackensack, NJ, 2005.
[5] A. Destexhe, A. Babloyantz, and T. J. Selnowski, *Ionic mechanisms for intrinsic slow oscillations in thalamic relay neurons*, Biophys. J., 65 (1993), pp. 1538–1552.
[6] A. Destexhe, D. A. McCormick, and T. J. Selnowski, *A model for* 8–10 *Hz spindling in interconnected thalamic relay and reticularis neurons*, Biophys. J., 65 (1993), pp. 2473–2477.
[7] J. D. Drover and B. Ermentrout, *Nonlinear coupling near a degenerate Hopf (Bautin) bifurcation*, SIAM J. Appl. Math., 63 (2003), pp. 1627–1647.
[8] B. Ermentrout, *Simulating, Analyzing, and Animating Dynamical Systems: A Guide to XPPAUT for Researchers and Students*, Software Environ. Tools 14, SIAM, Philadelphia, 2002.
[9] G. B. Ermentrout and N. Kopell, *Parabolic bursting in an excitable system coupled with a slow oscillation*, SIAM J. Appl. Math., 46 (1986), pp. 233–253.
[10] M. Golubitsky, K. Josić, and L. Shiau, *Bursting in coupled cell systems*, in Bursting, The Genesis of Rhythm in the Nervous System, World Scientific Publishing, Hackensack, NJ, 2005, pp. 201–221.
[11] E. M. Izhikevich, *Neural excitability, spiking and bursting*, Internat. J. Bifur. Chaos Appl. Sci. Engrg., 10 (2000), pp. 1171–1266.
[12] E. M. Izhikevich, *Synchronization of elliptic bursters*, SIAM Rev., 43 (2001), pp. 315–344.
[13] E. M. Izhikevich, *Resonance and selective communication via bursts in neurons having subthreshold oscillations*, BioSystems, 67 (2002), pp. 95–102.
[14] E. M. Izhikevich, *Dynamical Systems in Neuroscience: The Geometry of Excitability and Bursting*, MIT Press, Cambridge, MA, 2007.
[15] Y. A. Kuznetsov, *Elements of Applied Bifurcation Theory*, 3rd ed., Appl. Math. Sci. 112, Springer-Verlag, New York, 2004.
[16] C. D. Negro, C.-F. Hsiao, S. Chandler, and A. Garfinkel, *Evidence for a novel mechanism in rodent trigeminal neurons*, Biophys. J., 75 (1998), pp. 174–182.
[17] A. I. Neishtadt, *Prolongation of the loss of stability in the case of dynamic bifurcations.* I, Differential Equations, 23 (1987), pp. 1385–1390.
[18] A. I. Neishtadt, *Prolongation of the loss of stability in the case of dynamic bifurcations.* II, Differential Equations, 24 (1988), pp. 171–176.
[19] C. M. Pedroarena, I. E. Pose, J. Yamuy, M. H. Chase, and F. R. Morales, *Oscillatory membrane potential activity in the soma of a primary afferent neuron*, Neurophysiol., 82 (1999), pp. 1465–1476.
[20] M. I. Rabinovich, P. Varona, A. I. Selverston, and H. D. I. Abarbanel, *Dynamical principles in neuroscience*, Rev. Modern Phys., 78 (2006), pp. 1213–1265.
[21] J. Rinzel, *A formal classification of bursting mechanisms in excitable systems*, in Mathematical Topics in Population Biology, Morphogenesis and Neurosciences (Kyoto, 1985), Lecture Notes in Biomath. 71, Springer, Berlin, 1987, pp. 267–281.
[22] J. Rinzel and Y. S. Lee, *Dissection of a model for neuronal parabolic bursting*, J. Math. Biol., 25 (1987), pp. 653–675.

[23] J. Schwarz, G. Dangelmayr, A. Stevens, and K. Bräuer, *Burst and spike synchronization of coupled neural oscillators*, Dyn. Syst., 16 (2001), pp. 125–156.
[24] A. Sherman, *Anti-phase, asymmetric and aperiodic oscillations in excitable cells—I. Coupled bursters*, Bull. Math. Biol., 56 (1994), pp. 811–835.
[25] J. Su, J. Rubin, and D. Terman, *Effects of noise on elliptic bursters*, Nonlinearity, 17 (2004), pp. 133–157.